

Seismicity near the eastern Denali fault from temporary and long-term seismic recordings

Jongwon Han

Department of Earth and Environmental Sciences, Korea University, Seoul, Republic of Korea

Jan Dettmer*, Jeremy M. Gosselin, Hersh Gilbert and Katherine Biegel

Department of Geoscience, University of Calgary, Calgary, Alberta, Canada

Seongryong Kim

Department of Earth and Environmental Sciences, Korea University, Seoul, Republic of Korea

Han, J., Dettmer, J., Gosselin, J.M., Gilbert, H., Biegel, K. and Kim, S., 2024. Seismicity near the eastern Denali fault from temporary and long-term seismic recordings. In: Yukon Exploration and Geology Technical Papers 2023, L.H. Weston and Purple Rock Inc. (eds.), Yukon Geological Survey, p. 37–50.

Abstract

We studied earthquakes near Burwash Landing, Yukon. Using data from temporary and permanent seismic stations, we enhanced the understanding of both regional and local earthquakes. The study used deep learning and template matching to effectively detect earthquakes, even from noisy data. Following detection, seismic parameters, earthquake location, and magnitude were estimated and refined. The analysis revealed 103 local earthquakes, with 28 located in an area of geothermal resource potential. Notable small-magnitude earthquakes were observed near Bock's Creek fault. No earthquakes were observed on the Denali fault during the study period. The existence of active faults strike-parallel to the Denali fault suggests that local permeable structures may exist in the area. Regional observations detected 46 432 regional earthquakes in 13 years, but none along a section of the Denali fault near Burwash Landing, Yukon, which we interpret as a seismic gap.

Introduction

Southwestern Yukon exhibits complex active tectonism and significant earthquake activity due to plate boundary interactions between the Pacific and North American plates (Fig. 1). Major plate boundary structures in the region include the Queen Charlotte–Fairweather fault system, which has a primarily right-lateral strike-slip motion resulting from the oblique convergence of the Pacific Plate with the North American Plate and the Yakutat microplate (Leonard et al., 2007). The convergence is partitioned between the Aleutian Trench subduction zone, and a series of right-lateral, crustal strike-slip faults that includes the Denali fault zone (DFZ). Together, these features exemplify the diverse tectonic regime.

The Denali fault is a crustal-scale, dextral, strike-slip fault resulting from terrane accretion. It extends more than 2000 km from British Columbia through Yukon and central Alaska to the Bering Sea. The Denali fault has experienced right-lateral displacement of 400–480 km (Lowey, 1998; Waldien et al., 2021). Grantz (1966) partitions the Denali fault into three parts: the western segment in west-central Alaska, the central (McKinley) segment in eastern Alaska, and the eastern segment in southwestern Yukon. During the Holocene, fault activity was predominantly concentrated on the central McKinley segment, with additional activity on the southern Totschunda fault (Lanphere, 1978). The Denali fault has been a focus of recent seismic studies following the 2002 magnitude 7.9 Denali earthquake,

* jan.dettmer@ucalgary.ca

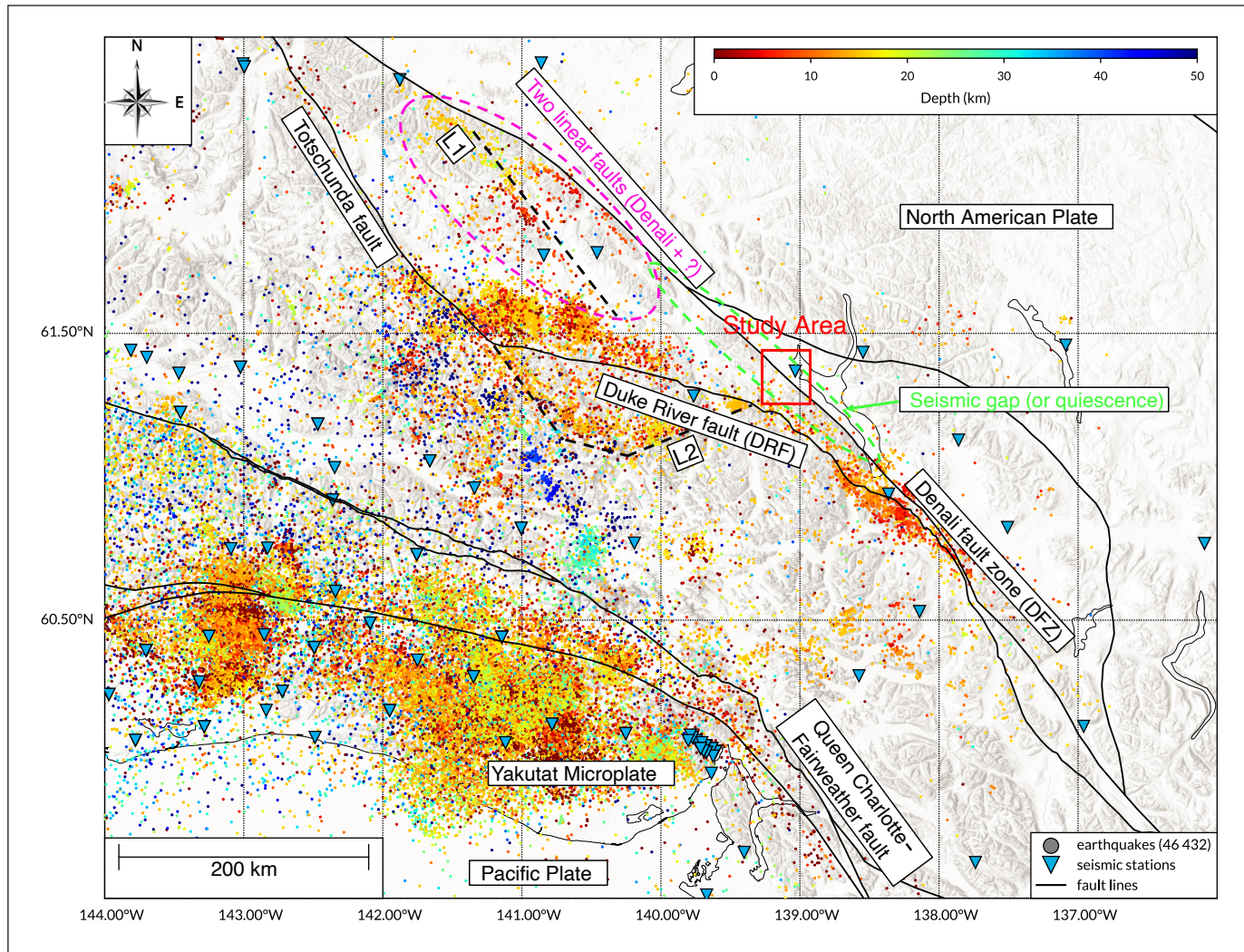


Figure 1. Regional distribution of earthquakes recorded between 2010 and 2023 near the study area (red rectangle) based on network data. The colour scale indicates event depths and highlights the predominantly shallow deformation along the Denali fault zone (DFZ). The dashed line labelled L1 represents the newly discovered linear seismic trend from this study; L2 is a lineament confirmed in previous studies (Biegel et al., 2023; Gosselin et al., 2023). Areas of particular interest are highlighted by dashed ellipses.

which highlighted the current seismic potential and complex rupture behaviour of past large events (Eberhart-Phillips et al., 2003).

Knowledge of the regional patterns of seismicity in southwestern Yukon was previously limited by sparse seismic network coverage, which has improved in recent years. The enhanced monitoring capabilities have facilitated a new understanding of regional seismicity and crustal stress regimes. Advances in seismic station deployment have expanded detection capabilities and improved precision in earthquake location and characterization, providing insight into the tectonic processes that shape the region (Meighan et al., 2013;

Ruppert and West, 2020; Biegel et al., 2023; Gosselin et al., 2023).

Regional seismicity is influenced by several fault systems including the Chugach-St. Elias, Fairweather, Denali and Teslin faults. These faults contribute to a complex pattern of seismicity, with events predominantly featuring reverse and dextral strike-slip mechanisms (L2 in Fig. 1; Gosselin et al., 2023). Notably, seismicity near the Duke River fault (DRF) zone exhibits mostly reverse faulting within a predominantly transpressive regional context, underscoring the diverse nature of fault behaviour in the area (Doser, 2014). In the St. Elias region, a combination of thrust and strike-slip fault

characteristics underscore the area (Plafker et al., 1978; Fletcher and Freymueller, 2003; Elliott et al., 2010). The St. Elias Mountains, a wide mountain range formed from multiple accreted terranes, are a testament to ongoing subduction processes, marking a zone of significant crustal seismicity between the Fairweather and Denali faults.

Recent research has focused on understanding the broader implications of these tectonic interactions. For instance, the behaviour of the Denali fault system is indicative of not just local, but also regional geodynamic processes. Specifically, the eastern segment of the Denali fault was hypothesized to serve as a regional stress boundary that influences seismic activity and deformation patterns of the adjacent areas (Choi et al., 2021). This perspective is critical for assessing the seismic hazard of the region and for understanding the broader tectonic framework of southwestern Yukon. The tectonic history and current dynamics of the Denali fault system offer insights into the potential for natural resource development in the region.

Southwestern Yukon is of particular interest for potential geothermal resource development (Majorowicz and Grasby, 2014); however, understanding the dynamic geological processes that characterize the resources and natural hazards is important for exploration and development. Regionally, the estimation of shallow Curie point depths (Li et al., 2017; Witter et al., 2018), shallow seismogenic crustal thickness (Biegel et al., 2023), and the mapping of radiogenic rocks and warm water springs, suggest significant geothermal potential in the region (Colpron, 2019). Locally, near Burwash Landing, shallow conductors were recently inferred from magnetotelluric data, which may be evidence for crustal fluid circulation in the vicinity of the Denali fault (Tschorhart et al., 2022). In this study, we present preliminary investigations of seismic patterns regionally (throughout southwestern Yukon) and locally near the eastern Denali fault (in the vicinity of Burwash Landing). The goal of this research is to improve knowledge of past and current regional tectonics, fault structure, and local behaviour near Burwash Landing, for the purpose of characterizing geothermal resource potential.

This paper presents preliminary results from a deep-learning-based earthquake detection algorithm (Mousavi et al., 2020) and a template-matching method

(Chamberlain et al., 2018) used to detect earthquakes below the noise thresholds of conventional analysis techniques. Regionally, we present the distribution of 46 432 earthquakes between 2010 and 2023, many of which are additions to the existing regional catalogue. Locally, we analyzed data from recent temporary seismic instrument deployments near Burwash Landing to identify 103 earthquakes. Specifically, we present 28 new earthquake locations, with associated magnitude estimates, near the Denali fault (DF). These newly identified events were detected from 8 weeks of recordings on a high-density linear nodal geophone array operated by the University of Calgary between June and August 2022. Notably, these events were detected over this short period in an area where earthquakes had not previously been observed in the decades-long record of regional seismic networks. Using magnitude-frequency analysis and waveform similarity clustering, we estimated source parameters of the earthquakes to characterize seismic events in the area. We also compared the local results to the long-term regional distribution of earthquakes from similar analyses of data from permanent stations in the region.

Our results show that the eastern Denali fault is seismically quiescent near Burwash Landing. However, other portions of the Denali fault exhibit significant seismicity. We interpreted these observations as the presence of a seismic gap on the eastern Denali fault with potential for future earthquakes. Active deformation on strike-parallel faults is evidence of permeable structures that may enable warm fluid mobility in the subsurface and improve prospects for geothermal potential. In combination with geophysical knowledge from recent studies, the improved understanding of seismicity from this work highlights geological complexity at regional and local scales. This further underscores the significance of the region for geothermal resource potential and the need for natural hazard assessments.

Method and data

Deep-learning-based earthquake detection and phase picker

We used EQTransformer (EQT), a deep-learning model for detecting earthquakes and identifying their seismic phases from continuous waveform data (Mousavi

et al., 2020). This model combines a long short-term memory (LSTM) network with a deep convolutional neural network (CNN) architecture comprising 56 layers. The LSTM is useful in handling sequential data (specifically processing longer sequences). The deep CNN architecture in EQT uses convolutional layers coupled with max pooling, a common approach in deep-learning models to reduce the spatial dimensions of data while retaining important features. To address the potential degradation issues associated with deep CNNs, especially when strong downsampling is involved, EQT uses residual connections within the CNN. These connections help preserve information throughout the network, ensuring the integrity of the input data from beginning to end.

EQTransformer incorporates an attention mechanism, a feature that enhances the model's ability to extract core features by focusing on local aspects (e.g., individual seismic phases) and the overall context (e.g., an entire wave packet containing body and surface waves). This mechanism plays a crucial role in estimating probabilities in three key areas of the model: earthquake full waveform, P-wave phase and S-wave phase detection. The output from each of these areas is processed through a sigmoid layer, which produces a probability distribution on [0,1]. These probabilities are used as threshold values to classify input signals as earthquakes. For practical application, specific threshold values used in a previous study (Mousavi et al., 2020) were set for the detection of P-waves, S-waves and earthquakes at 0.3, 0.1 and 0.1, respectively.

The original model was trained on the STanford EArthquake Dataset (STEAD), which consists of approximately 1 000 000 records of local earthquakes and 300 000 noise signals (Mousavi et al., 2019). Generally, instead of starting learning from scratch, retraining based on an existing model can yield a training model optimized for the research area. In this study, we also conducted transfer learning using earthquake origin information and phase-picking data from Biegel et al. (2023), which led to the development of a model that is finely tuned for our research area near Burwash Landing. The model's comprehensive structure, with 372 000 parameters across its 56-layer network, highlights its complexity and capability in earthquake detection and phase identification.

Template-matching-based earthquake detection

In recent research, initial earthquake catalogues have been constructed through a deep learning-based approach, followed by detecting additional earthquakes based on the similarity of event waveforms (i.e., template-matching techniques; Chamberlain et al., 2018). The template-matching technique uses an event waveform as a template to search for similar waveforms in continuous data. This technique is effective for detecting earthquakes using continuous seismic data and a template waveform. It relies on the similarity of waveforms from different events recorded on the same seismograph, provided these events originate from nearby locations, have similar rupture mechanisms and share similar paths from their sources to the receivers. The advantage of template matching is its ability to detect earthquakes in noisy data, where traditional methods fail.

A significant drawback of the template-matching technique is computational cost, exacerbated by the increasing number of templates and the volume of continuous data that must be analyzed. Recent technical advancements, particularly in the use of graphics processing units (GPUs), have been instrumental in mitigating this issue, as pointed out by Beaucé et al. (2017). The use of GPUs enhanced the efficiency of the template-matching technique, enabling the detection of up to 20 times more events than traditional processing technologies while significantly reducing computation time. This is a considerable improvement in earthquake detection capability, particularly in identifying small-scale events that were previously undetectable with older methods. In this study, we used the match and locate method (Liu et al., 2020) to calculate waveform similarity within a GPU setting.

Estimation of earthquake source parameters

After detecting earthquakes, the initial locations are determined using HYPOELLISE (Lahr, 1999), a software program designed for earthquake location using 1D seismic velocity model. Central to this method is the calculation of seismic wave traveltimes, which depends on a 1D seismic velocity model. The program calculates earthquake locations by iteratively refining the estimated hypocentre location and origin

time using the arrival times of P-waves and S-waves recorded at multiple stations. HYPOELLIPE uses least squares inversion to minimize the difference between observed and calculated arrival times, thereby optimizing the hypocentre estimate. In this study, we used a 1D velocity model presented in Fogleman et al. (1993). Following initial location, we relocated events with the double-difference method (Waldhauser and Ellsworth, 2000), which improves the accuracy of hypocentres for earthquakes that occur in proximity to each other. It compares differences in traveltimes and waveform similarities between pairs of earthquakes recorded by the same seismic station. By focusing on these relative time differences instead of absolute traveltimes, the method effectively minimizes the effects of heterogeneous velocity structures in the Earth's crust. Using the waveform similarities, the method groups the earthquakes based on cross-correlation coefficients (CC) between event pairs and uses this information during the iterations for locating hypocentres. This leads to more precise hypocentre locations, especially in regions with complex geological structures. Finally, we converted all waveforms to Wood-Anderson amplitudes (Uhrhammer and Collins, 1990), and estimated local magnitudes based on the equation suggested by Fogleman et al. (1993).

Data

We analyzed data from 34 temporary seismic stations (nodal geophones) that form two linear arrays crossing the Denali fault near Burwash Landing (Fig. 2) on transects that follow Burwash Creek and the Duke River. The stations operated from June 14 to August 22, 2022. The geophones have a natural frequency of 5 Hz, making them ideal for detecting local earthquakes of small magnitude. To investigate earthquakes at the regional scale, we used data from permanent International Federation of Digital Seismograph Network (FDSN) stations, accessed through Incorporated Research Institutions for Seismology (IRIS; see data and resources section). Regional earthquake data processing followed the same steps using the framework suggested by Han et al. (2023). All data were bandpass filtered to a range of 1–45 Hz. For the template matching and waveform similarity clustering analyses, which targeted the S-wave phase, a narrower bandpass filter range of 2–15 Hz was applied.

Results and discussion

Local seismicity near Burwash Landing

We studied an area near Burwash Landing, Yukon (Fig. 2). Notably, this is an area that has shown few earthquakes in the past 15 years, despite significant improvements in instrumentation coverage (Fig. 2). The earthquakes presented here were identified by applying the deep-learning model to geophone data, followed by detection of micro-earthquakes using template matching. All earthquakes detected by the deep-learning picker were used as template waveforms and applied as continuous waveforms to estimate CC. Following each earthquake detection, initial locations were determined using HYPOELLIPE (Lahr, 1999), and then redetermined using HypoDD (Waldhauser and Ellsworth, 2000) using the estimated CCs. This process identified 103 earthquakes, ranging in magnitude from 0.6 to 3.1. We located 75 earthquakes within the study area (Fig. 3). Using magnitude-frequency analysis, the magnitude of completeness of the presented catalogue was determined to be 1.1, and the b-value was found to be 0.94 (Fig. 4), which is similar to global averages.

Although the short observation period limits the interpretation of earthquake trends from these data alone, we identified three spatially distinct groups (Fig. 3). Group 2 (Fig. 5) occurred near Burwash Landing and includes earthquakes close to, but not on, the Denali fault. These events are not reported by the United States Geological Survey (USGS) catalogue (see data and resources section for more details). Group 2a includes earthquakes related to the DRF. Group 2b includes events we interpreted to be on Bock's Creek fault (BCF), and on faults that appear to accommodate deformation connecting BCF to other faults previously inferred from digital elevation models (Witter, 2020) and lidar surveys (Finley et al., 2022). In the Group 2a area, fault plane solutions from catalogued earthquakes outside deployment time for our data have northwest strikes (Doser, 2014; Gosselin et al., 2023) and reverse fault motion; however, the DRF is a southwest-dipping thrust fault, and the observed earthquakes appear on the footwall, suggesting that they may occur in an unmapped fault developing between the DRF and DF, similar to the BCF.

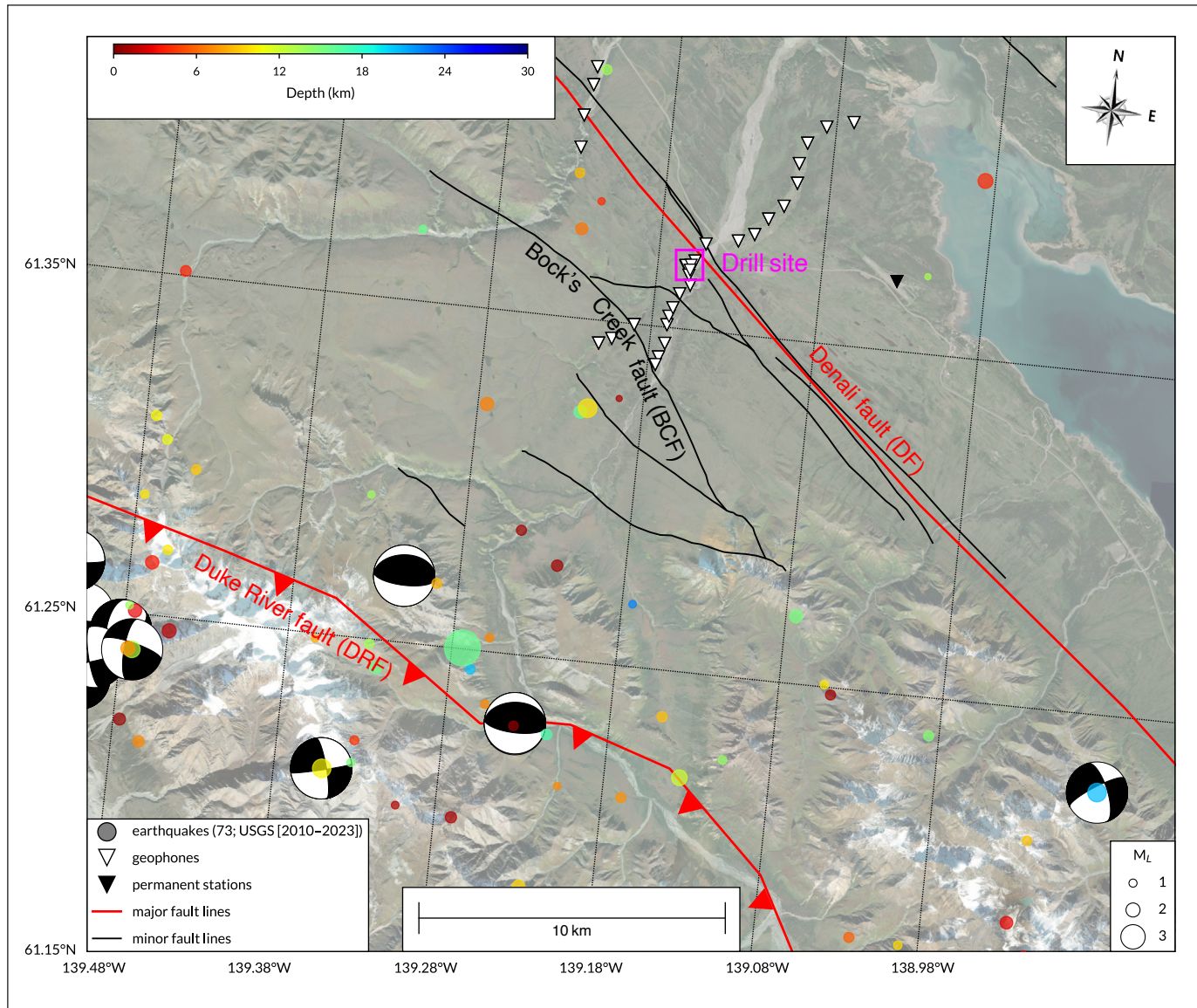


Figure 2. Distribution of geophone array stations (white triangles) and earthquakes reported by the United States Geological Survey between 2010 and 2023 within the study area. Note the absence of earthquakes along the Denali fault (DF). A small number of earthquakes were observed near Bock's Creek fault (BCF). M_L : Richter local magnitude of earthquakes observed. The drill site marks the location of an approximately 200 m deep exploratory well installed by the Yukon Geological Survey. The focal mechanisms for earthquakes contained in the USGS catalogue are also shown.

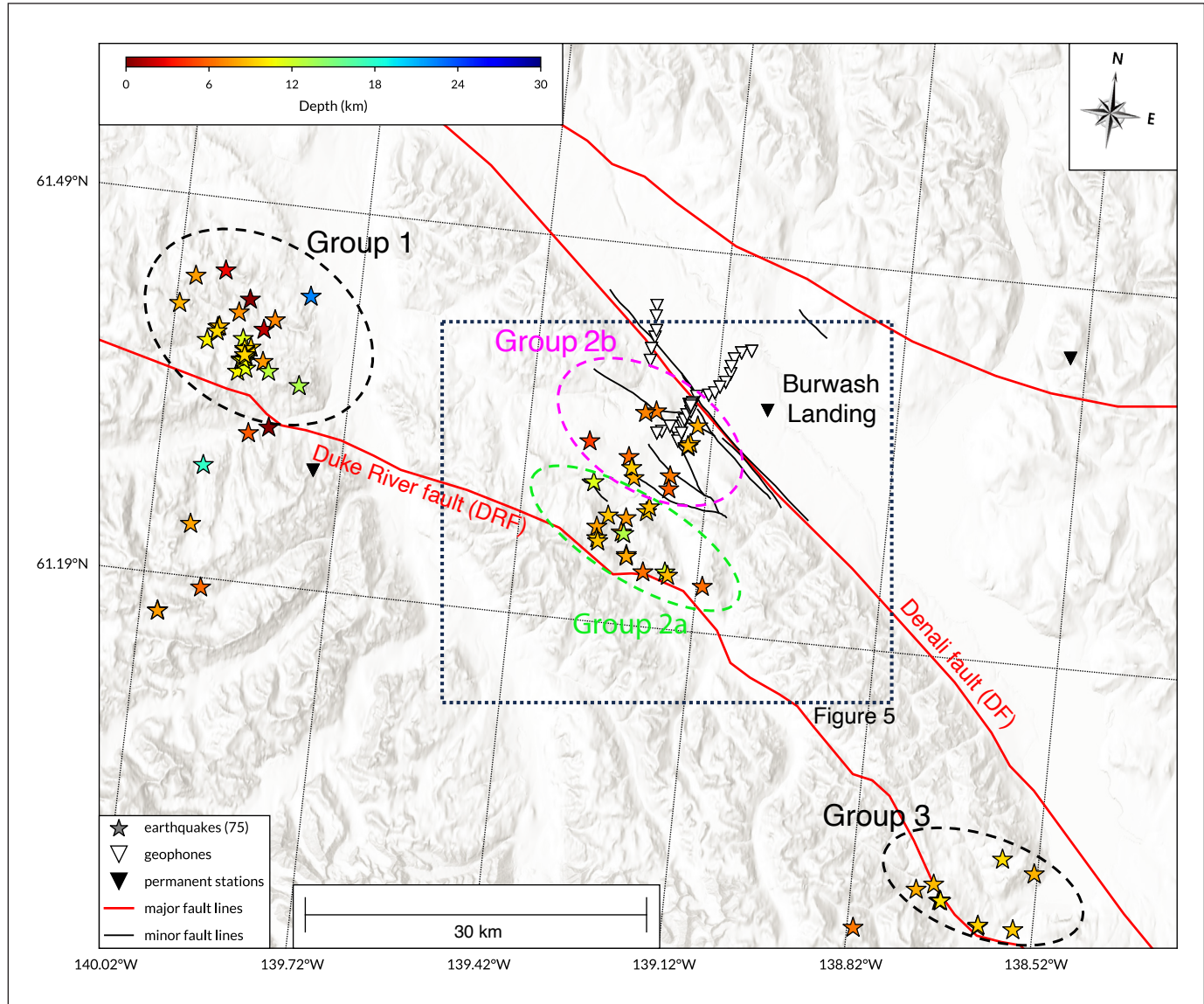


Figure 3. Earthquakes (stars) detected in the study area as part of this study. Colours of stars indicate earthquake depths. Seismicity clusters in three groups are highlighted by ellipses. The dashed rectangle outlines the area presented in further detail in Figure 5.

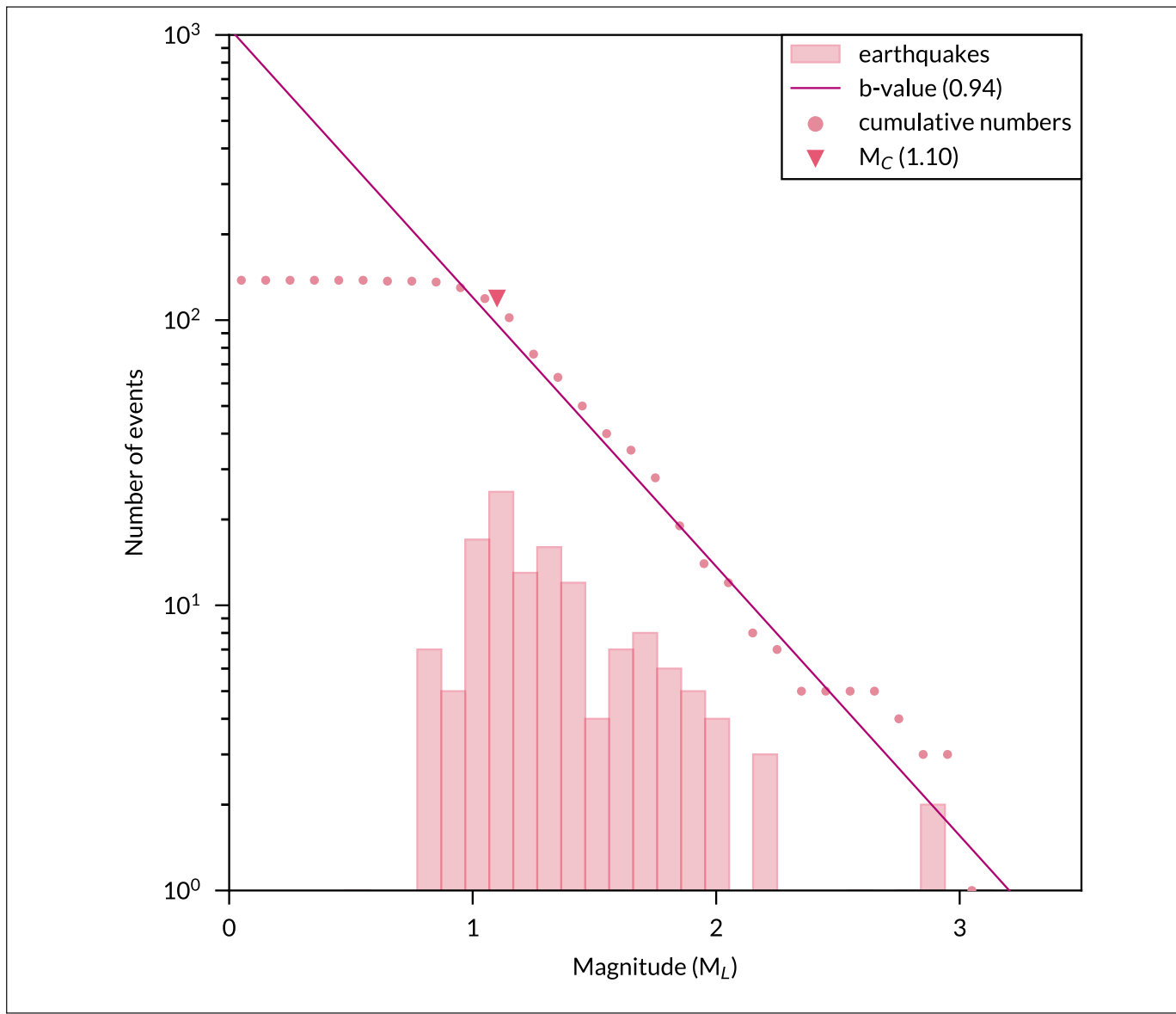


Figure 4. Gutenberg-Richter analysis of the local earthquake catalogue showing a power-law distribution of earthquake frequency with magnitude (M_L) that is typical of global active tectonic settings. The magnitude of completeness (M_C) value is also shown.

To cluster these earthquakes, an event dendrogram was determined by analyzing waveform similarity using station 32 from the temporal seismic array, which provided the most phase information among the detected results (Fig. 6). The earthquake clusters were divided into eight groups (C1–C8). Waveform-similarity-based analysis identified earthquake clusters C3 and C4, which are related to Group 2b (Fig. 7). Cluster C4 is distributed closer to the geophone array compared to C3, with differing waveform characteristics (Fig. 7). The C3 events are located to the southwest of the seismic network, suggesting a

possible origin from a minor fault between strands of BCF (Fig. 7). The two events of C3 may be located on the same portion of BCF or, alternatively, come from an unmapped fault connecting these fault strands (Fig. 7). This possible unmapped fault may be related to those previously identified by the inversion of three passive electromagnetic datasets (Tschorhart et al., 2022). Although the precision of our interpretations is limited by the scarcity of data and the aperture of the seismic network, this study confirms active deformation, with earthquakes occurring on smaller fault structures in the area. The absence of microearthquakes on the Denali

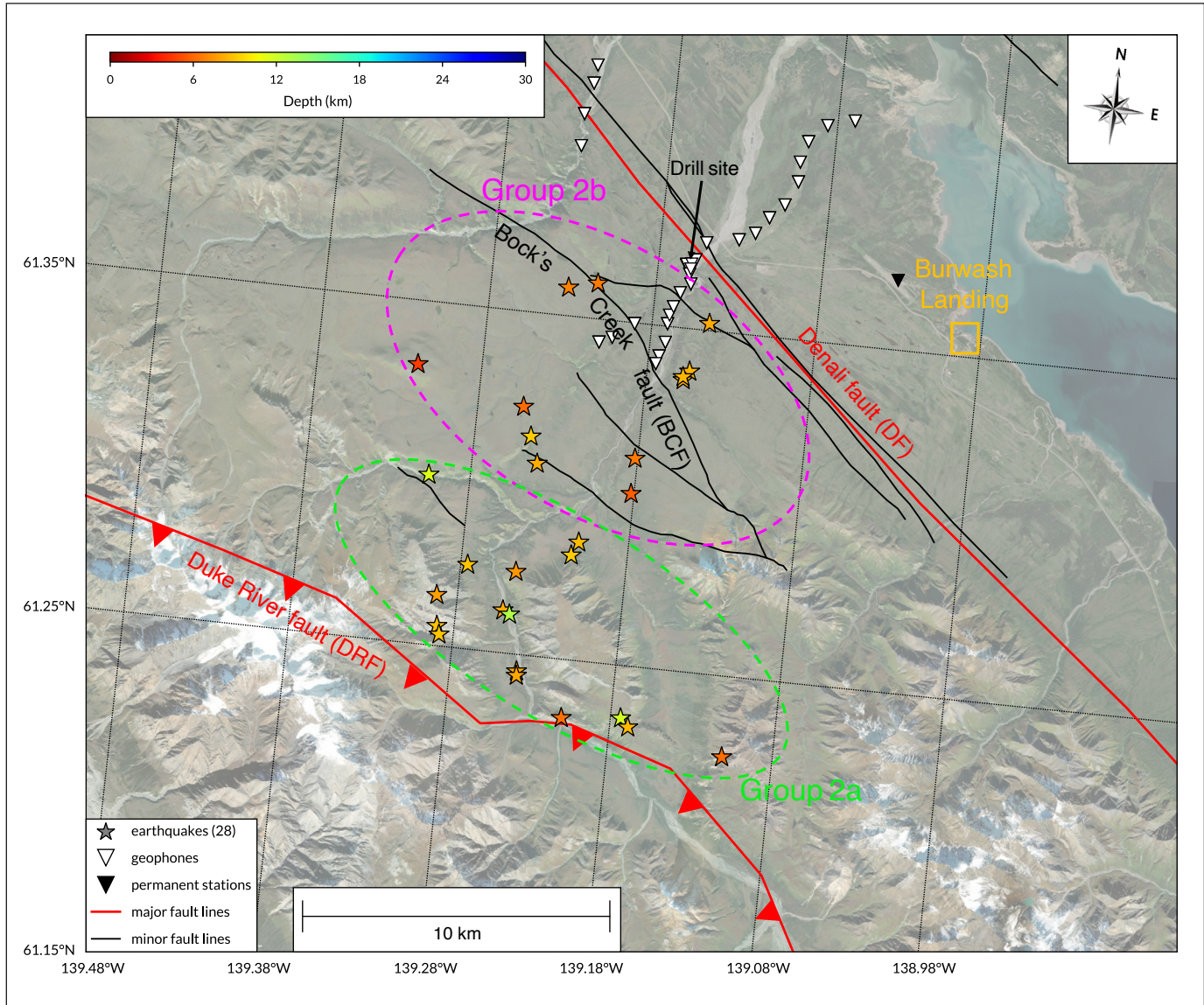


Figure 5. Detailed view of earthquakes near Burwash Landing, Yukon. Group 2a occurs on the footwall of the Duke River fault (DRF), and may have originated from an unmapped fault between the DRF and the Denali fault (DF). Group 2b is of particular interest because it includes 13 earthquakes consistent with recently mapped faults, the Bock's Creek fault (BCF) and other related fault structures (Witter, 2020; Finley et al., 2022).

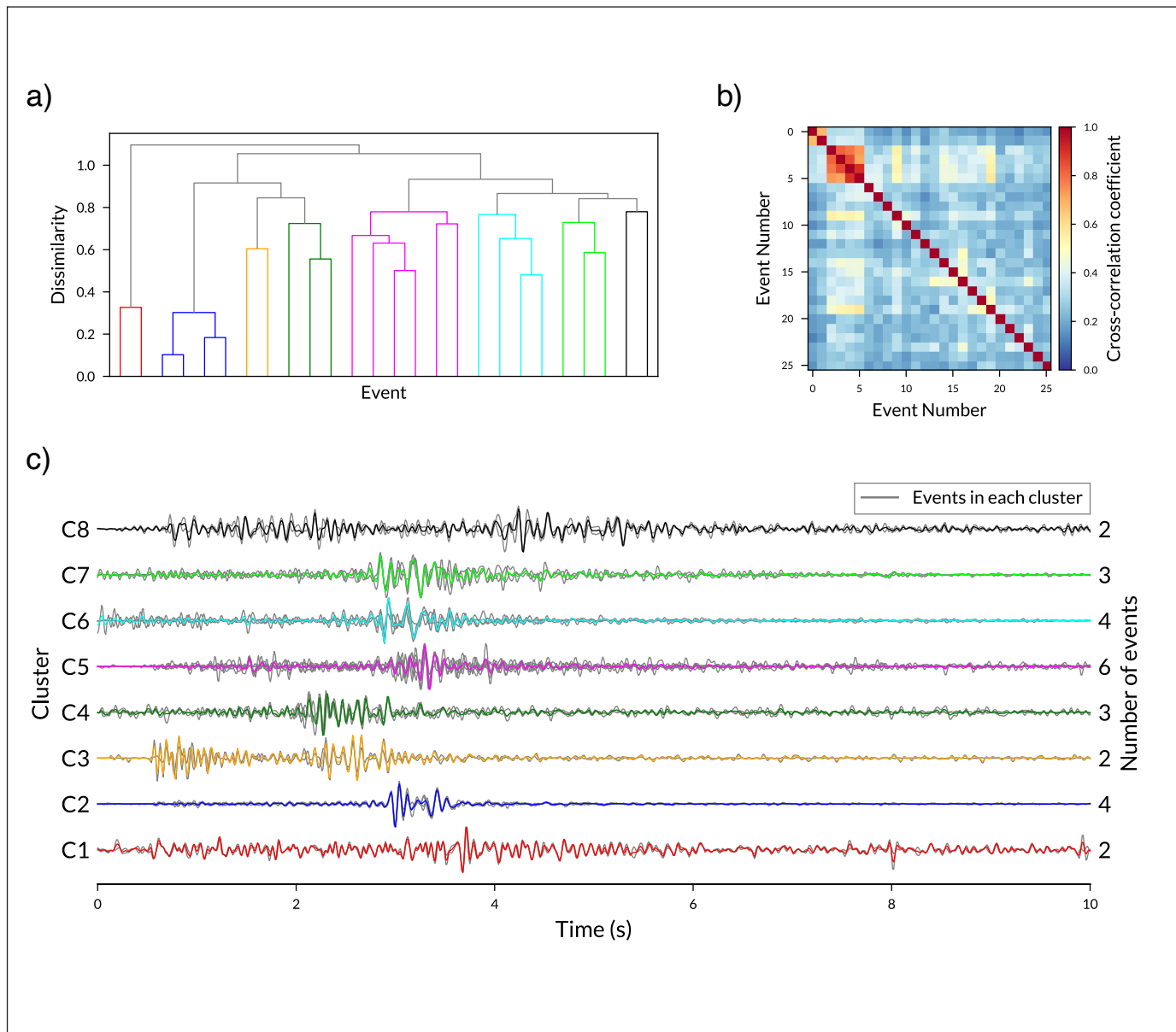


Figure 6. Analysis of waveform similarity for the earthquake events shown in Figure 5: **a)** dendrogram of earthquakes based on waveform similarity; **b)** cross-correlation coefficient matrix between event pairs; **c)** individual (grey lines) and stacked (coloured lines) waveforms of clustered earthquakes.

fault is peculiar and provides evidence of a seismic gap, considering that regional networks have also not detected earthquakes in this location.

Regional seismicity

We also present an extended catalogue of more than 40 000 earthquakes at the regional scale, based on continuous seismic data of permanent stations, that significantly extends the USGS catalogue (see data and resources section for more details). Detection and

phase picking were conducted in the same manner as previously discussed (Han et al., 2023). Phase association was calculated using a Bayesian-Gaussian mixture model (Zhu et al., 2022). The results show 46 432 regional earthquakes between 2010 and 2023 (Fig. 1). A detailed interpretation of this catalogue is not the focus of this report. Broadly speaking, the distribution of these earthquakes supports the interpretation proposed by Biegel et al. (2023) and identifies linear structures not previously reported. Most important to this study is the observed lack of

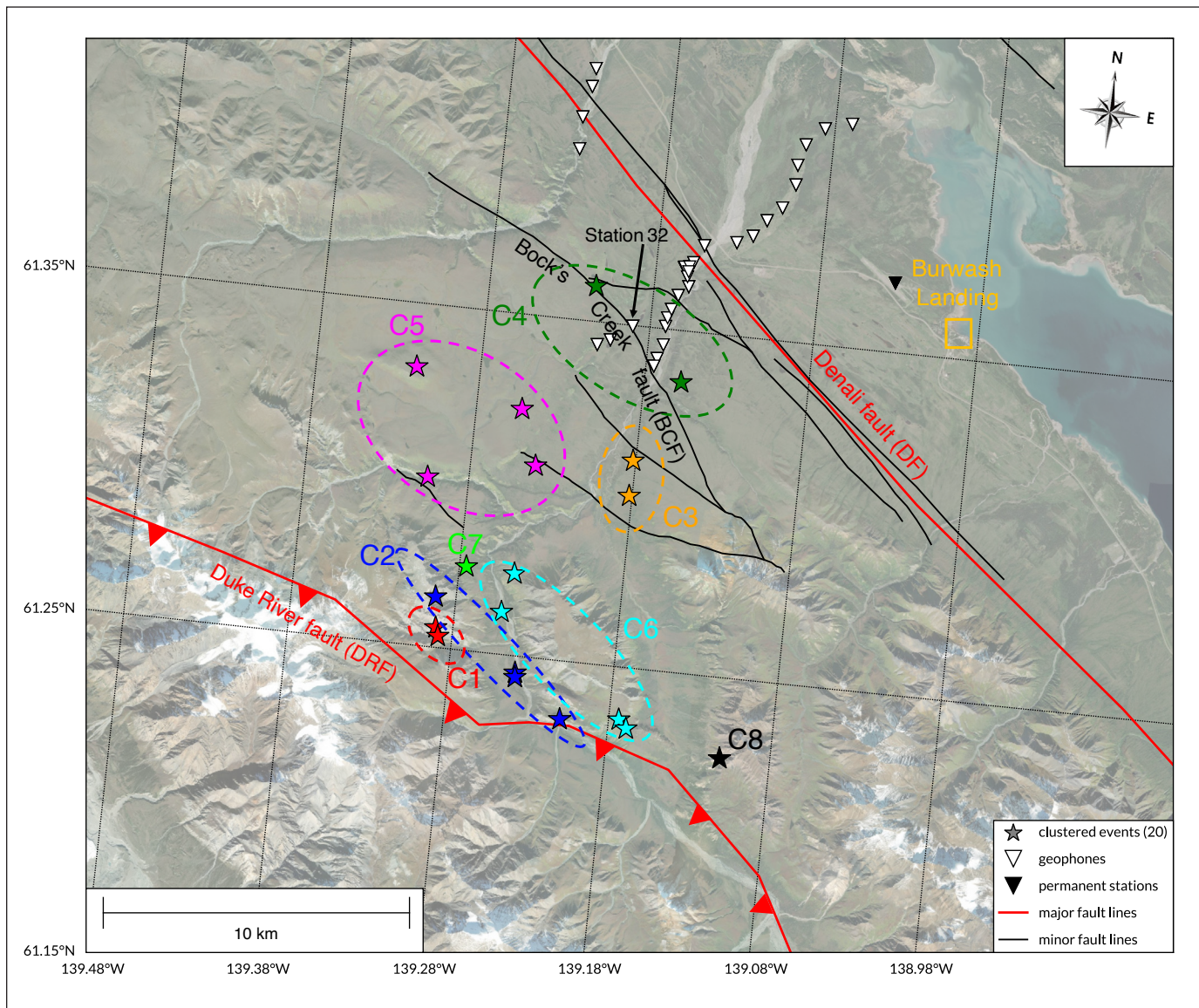


Figure 7 Map of clustered events in Figure 6. The events in each cluster (C1–C8) exhibit highly similar waveforms suggesting that these earthquakes occur on the same structures.

seismicity in the vicinity of the DFZ in a 50–100 km long fault section near Burwash Landing, which may present a seismic gap with increased potential for future earthquakes.

A second observation of interest is located farther northwest (Fig. 1). Here, a distinct linear trend parallel to the Denali fault is observed that was not previously reported (L1 in Fig. 1). The newly interpreted parallel fault segment southwest of the main Denali fault appears to connect to the DRF zone as discussed in Gosselin et al. (2023).

Conclusion

This paper presents a detailed seismic analysis of southwestern Yukon, highlighting the seismicity near Burwash Landing. Using a combination of data collected from temporary seismic stations operated during summer 2022 and long-term data from permanent stations, we offer new insights into the seismicity of this geologically complex region. Key findings include the identification of 46 432 regional earthquakes from a decade-long period and 103 local earthquakes from a three-month period. The study effectively used advanced seismic detection techniques

such as deep-learning-based earthquake detection and template matching to enhance earthquake catalogue completeness and accuracy. The application of HYPOELLIPE and HypoDD provided refined hypocentre locations and magnitude estimations, contributing to a more comprehensive understanding of the seismic behaviour in the area. Regionally, we have identified new linear seismic structures and added to the existing knowledge of the tectonic framework through this study. While the study had limitations, such as the short observation period and small aperture of the temporary array, the research significantly advances our understanding of the seismicity and tectonic processes near the eastern Denali fault and Burwash Landing area. Specifically, we observed no seismicity associated with the eastern Denali fault, which we interpreted as a seismic gap. Additionally, we observed that active deformation occurs on strike-parallel fault structures which may increase rock permeability. These observations highlight the significance of the region in terms of both geothermal resource potential and the need for natural hazard assessments.

Data and resources

Seismograms from permanent stations used in this study were collected from the Incorporated Research Institutions for Seismology Data Management Centre (IRIS, 2023). The earthquake catalogue used is published by the United States Geological Survey (USGS, 2023). All maps were obtained from ArcGIS REST API services (ArcGIS, 2023). The local and regional earthquake catalogues, including local magnitudes for the local catalogue, are available as a data supplement to this paper in comma-separated values format.

Acknowledgments

We respectfully acknowledge that the data for this study were recorded in the Traditional Territory of the Kluane First Nation. This work was funded by the Yukon Geological Survey (YGS); Natural Sciences and Engineering Research Council of Canada Alliance Grant ALLRP-580887-22; and by the Natural Science and Engineering Research Council of Canada through Discovery Grants to Jan Dettmer and Hersh Gilbert and a postdoctoral fellowship to Jeremy Gosselin. We thank Maurice Colpron from YGS for helpful discussions.

References

- ArcGIS (2023): ArcGIS REST services directory. Version 10.91. <https://server.arcgisonline.com/arcgis/rest> [accessed December 2023].
- Beaucé, E., Frank, W.B. and Romanenko, A., 2017. Fast matched filter (FMF): An efficient seismic matched-filter search for both CPU and GPU architectures. *Seismological Research Letters*, vol. 89, no. 1, p. 165–172. <https://doi.org/10.1785/0220170181>
- Biegel, K., Gosselin, J. and Dettmer, J., 2023. Preliminary double-difference relocation earthquake catalogue for southwestern Yukon centred along the Denali fault zone. In: Yukon Exploration and Geology 2022, K.E. MacFarlane (ed.), Yukon Geological Survey, p. 1–18, plus digital appendices.
- Chamberlain, C.J., Hopp, C.J., Boese, C.M., Warren-Smith, E., Chambers, D., Chu, S.X., Michailos, K. and Townend, J., 2018. EQcorrscan: Repeating and near-repeating earthquake detection and analysis in Python. *Seismological Research Letters*, vol. 89, no. 1, p. 173–181. <https://doi.org/10.1785/0220170151>
- Choi, M., Eaton, D.W. and Enkelmann, E., 2021. Is the eastern Denali fault still active? *Geology*, vol. 49, no. 6, p. 662–666. <https://doi.org/10.1130/G48461.1>
- Colpron, M., 2019. Potential radiogenic heat production from granitoid plutons in Yukon. Yukon Geological Survey, Open File 2019-16, 1 map and data.
- Doser, D.I., 2014. Seismicity of southwestern Yukon, Canada, and its relation to slip transfer between the Fairweather and Denali fault systems. *Tectonophysics*, vol. 611, p. 121–129. <https://doi.org/10.1016/j.tecto.2013.11.018>
- Eberhart-Phillips, D., Haeussler, P.J., Freymueller, J.T., Frankel, A.D., Rubin, C.M., Craw, P., Ratchkovski, N.A., Anderson, G., Carver, G.A. and Crone, A.J., 2003. The 2002 Denali fault earthquake, Alaska: A large magnitude, slip-partitioned event. *Science*, vol. 300, p. 1113–1118. <https://doi.org/10.1126/science.1082703>

- Elliott, J.L., Larsen, C.F., Freymueller, J.T. and Motyka, R.J., 2010. Tectonic block motion and glacial isostatic adjustment in southeast Alaska and adjacent Canada constrained by GPS measurements. *Journal of Geophysical Research: Solid Earth*, vol. 115, no. B9, article B09407, 21 p. <https://doi.org/10.1029/2009JB007139>
- Finley, T., Salomon, G., Stephen, R., Nissen, E., Cassidy, J. and Menounos, B., 2022. Preliminary results and structural interpretations from drone lidar surveys over the Eastern Denali fault, Yukon. In: *Yukon Exploration and Geology 2021*, K.E. MacFarlane (ed.), Yukon Geological Survey, p. 83–105.
- Fletcher, H.J. and Freymueller, J.T., 2003. New constraints on the motion of the Fairweather fault, Alaska, from GPS observations. *Geophysical Research Letters*, vol. 30, no. 3, article 1139, 4 p. <https://doi.org/10.1029/2002GL016476>
- Fogleman, K.A., Lahr, J.C., Stephens, C.D. and Page, R.A., 1993. Earthquake locations determined by the southern Alaska seismograph network for October 1971 through May 1989: United States Geological Survey, Open-File Report 93–309, 54 p. <https://doi.org/10.3133/ofr93309>
- Gosselin, J.M., Biegel, K., Hamidbeygi, M. and Dettmer, J., 2023. Improvements in the regional earthquake focal mechanism catalogue for southwestern Yukon. In: *Yukon Exploration and Geology 2022*, K.E. MacFarlane (ed.), Yukon Geological Survey, p. 63–76 plus digital appendices.
- Grantz, A., 1966. Strike-slip faults in Alaska: United States Geological Survey, Open-File Report 66–53, 82 p. <https://doi.org/10.3133/ofr6653>
- Han, J., Seo, K.J., Kim, S., Sheen, D.-H., Lee, D. and Byun, A.-H., 2023. Research catalog of inland seismicity in the southern Korean Peninsula from 2012 to 2021 using deep learning techniques. *Seismological Research Letters*. <https://doi.org/10.1785/0220230246>
- IRIS, 2023: Incorporated Research Institutions for Seismology Data Management Centre. <https://www.iris.edu> [accessed October 2023].
- Lahr, J.C., 1999. HYPOELLIPSE: A computer program for determining local earthquake hypocentral parameters, magnitude, and first-motion pattern: United States Geological Survey, Open-File Report 99–23, version 1.1, 119 p. and software. <https://pubs.usgs.gov/of/1999/ofr-99-0023/>
- Lanphere, M.A., 1978. Displacement history of the Denali fault system, Alaska and Canada. *Canadian Journal of Earth Sciences*, vol. 15, no. 5, p. 817–822. <https://doi.org/10.1139/e78-086>
- Leonard, L.J., Hyndman, R.D., Mazzotti, S., Nykolaishen, L., Schmidt, M. and Hippchen, S., 2007. Current deformation in the northern Canadian Cordillera inferred from GPS measurements. *Journal of Geophysical Research: Solid Earth*, vol. 112, no. B11, article B11401, 15 p. <https://doi.org/10.1029/2007JB005061>
- Li, C.-F., Lu, Y. and Wang, J., 2017. A global reference model of Curie-point depths based on EMAG2. *Scientific Reports*, vol. 7, article 45129. <https://doi.org/10.1038/srep45129>
- Liu, M., Li, H., Zhang, M. and Wang, T., 2020. Graphics processing unit-based match and locate (GPU-M&L): An improved match and locate method and its application. *Seismological Research Letters*, vol. 91, no. 2A, p. 1019–1029. <https://doi.org/10.1785/0220190241>
- Lowey, G.W., 1998. A new estimate of the amount of displacement on the Denali fault system based on the occurrence of carbonate megaboulders in the Dezadeash Formation (Jura-Cretaceous), Yukon, and the Nutzotin Mountains sequence (Jura-Cretaceous), Alaska. *Bulletin of Canadian Petroleum Geology*, vol. 46, no. 3, p. 379–386.
- Majorowicz, J. and Grasby, S.E., 2014. Geothermal energy for northern Canada: Is it economical? *Natural Resources Research*, vol. 23, no. 1, p. 159–173. <https://doi.org/10.1007/s11053-013-9199-3>
- Meighan, L.N., Cassidy, J.F., Mazzotti, S. and Pavlis, G.L., 2013. Microseismicity and tectonics of southwest Yukon Territory, Canada, using a local dense seismic array. *Bulletin of the Seismological Society of America*, vol. 103, no. 6, p. 3341–3346. <https://doi.org/10.1785/0120130068>

- Mousavi, S.M., Ellsworth, W.L., Zhu, W., Chuang, L.Y. and Beroza, G.C., 2020. Earthquake transformer—an attentive deep-learning model for simultaneous earthquake detection and phase picking. *Nature Communications*, vol. 11, article 3952. <https://doi.org/10.1038/s41467-020-17591-w>
- Mousavi, S.M., Sheng, Y., Zhu, W. and Beroza, G.C., 2019. Stanford Earthquake Dataset (STEAD): A global data set of seismic signals for AI. *IEEE access*. <https://doi.org/10.1109/ACCESS.2019.2947848>
- Plafker, G., Hudson, T., Bruns, T. and Rubin, M., 1978. Late Quaternary offsets along the Fairweather fault and crustal plate interactions in southern Alaska. *Canadian Journal of Earth Sciences*, vol. 15, no. 5, p. 805–816. <https://doi.org/10.1139/e78-085>
- Ruppert, N.A. and West, M.E., 2020. The impact of USArray on earthquake monitoring in Alaska. *Seismological Research Letters*, vol. 91, no. 2A, p. 601–610. <https://doi.org/10.1785/0220190227>
- Tschirhart, V., Colpron, M., Craven, J., Ghalati, F.H., Enkin, R.J. and Grasby, S.E., 2022. Geothermal exploration in the Burwash Landing region, Canada, using three-dimensional inversion of passive electromagnetic data. *Remote Sensing*, vol. 14, no. 23, article 5963. <https://doi.org/10.3390/rs14235963>
- Uhrhammer, R.A. and Collins, E.R., 1990. Synthesis of Wood-Anderson seismograms from broadband digital records. *Bulletin of the Seismological Society of America*, vol. 80, no. 3, p. 702–716.
- USGS, 2023: Earthquake catalog. Earthquake Hazards Program. USGS. <https://earthquake.usgs.gov/earthquakes/search/> [accessed November 2023].
- Waldhauser, F. and Ellsworth, W.L., 2000. A double-difference earthquake location algorithm: Method and application to the northern Hayward fault, California. *Bulletin of the Seismological Society of America*, vol. 90, no. 6, p. 1353–1368. <https://doi.org/10.1785/0120000006>
- Waldien, T., Roeske, S. and Benowitz, J., 2021. Tectonic underplating and dismemberment of the Maclaren-Kluane schist records Late Cretaceous terrane accretion polarity and ~480 km of post-52 Ma dextral displacement on the Denali fault. *Tectonics*, vol. 40, no. 10, article e2020TC006677. <https://doi.org/10.1029/2020TC006677>
- Witter, J.B., 2020. Early-stage exploration for geothermal energy resources along the Denali fault near Duke River, Yukon. Yukon Geological Survey, Open File 2020-3, 62 p.
- Witter, J.B., Miller, C.A., Friend, M. and Colpron, M., 2018. Curie point depths and heat production in Yukon, Canada. In: Proceedings, 43rd Workshop on Geothermal Reservoir Engineering, Stanford University, Standford, California, February 12-14, 2018 SGP-TR-213, p. 12–14.
- Zhu, W., McBrearty, I.W., Mousavi, S.M., Ellsworth, W.L. and Beroza, G.C., 2022. Earthquake phase association using a Bayesian Gaussian mixture model. *Journal of Geophysical Research: Solid Earth*, vol. 127, no. 5, article e2021JB023249. <https://doi.org/10.1029/2021JB023249>